Faculty Publications

2015

Characterization of the LIGO detectors during their sixth science run

Tiffany Summerscales
Andrews University, tzs@andrews.edu

LIGO Collaboration

Follow this and additional works at: https://digitalcommons.andrews.edu/pubs

Part of the Astrophysics and Astronomy Commons

Characterization of the LIGO detectors during their sixth science run

Characterization of the LIGO detectors during their sixth science run

J Aasi[1], J Abadie[1], B P Abbott[1], R Abbott[1], T Abbott[2],
M R Abernathy[1], T Accadia[3], F Acernese[4,5], C Adams[6],
T Adams[7], R X Adhikari[1], C Affeldt[8], M Agathos[9],
N Aggarwal[10], O D Aguiar[11], P Ajith[1], B Allen[8,12,13],
A Allocca[14,15], E Amador Ceron[12], D Amariutei[16],
R A Anderson[1], S B Anderson[1], W G Anderson[12], K Arai[1],
M C Araya[1], C Arceneaux[17], J Areeda[18], S Ast[13], S M Aston[6],
P Astone[19], P Aufmuth[13], C Aulbert[8], L Austin[1], B E Aylott[20],
S Babak[21], P T Baker[22], G Ballardin[23], S W Ballmer[24],
J C Barayoga[1], D Barker[25], S H Barnum[10], F Barone[4,5],
B Barr[26], L Barsotti[10], M Barsuglia[27], M A Barton[25], I Bartos[28],
R Bassiri[29,26], A Basti[14,30], J Batch[25], J Bauchrowitz[8],
Th S Bauer[9], M Bebronne[3], B Behnke[21], M Bejger[31],
M G Beker[9], A S Bell[26], C Bell[26], I Belopolski[28], G Bergmann[8],
J M Berliner[25], A Bertolini[9], D Bessis[32], J Betzwieser[6],
P T Beyersdorf[33], T Bhadbhade[29], I A Bilenko[34],
G Billingsley[1], J Birch[6], M Bitossi[14], M A Bizouard[35],
E Black[1], J K Blackburn[1], L Blackburn[36], D Blair[37], M Blom[9],
O Bock[8], T P Bodiya[10], M Boer[38], C Bogan[8], C Bond[20],
F Bondu[39], L Bonelli[14,30], R Bonnand[40], R Bork[1], M Born[8],
S Bose[41], L Bosi[42], J Bowers[2], C Bradaschia[14], P R Brady[12],
V B Braginsky[34], M Branchesi[43,44], C A Brannen[41],
J E Brau[45], J Breyer[8], T Briant[46], D O Bridges[6], A Brillet[38],
M Brinkmann[8], V Brisson[35], M Britzger[8], A F Brooks[1],
D A Brown[24], D D Brown[20], F Brückner[20], T Bulik[47],
H J Bulten[9,48], A Buonanno[49], D Buskulic[3], C Buy[27],
R L Byer[29], L Cadonati[50], G Cagnoli[40], J Calderón Bustillo[51],
E Calloni[4,52], J B Camp[36], P Campsie[26], K C Cannon[53],
B Canuel[23], J Cao[54], C D Capano[49], F Carbognani[23],
L Carbone[20], S Caride[55], A Castiglia[56], S Caudill[12],
M Cavaglià[17], F Cavalier[35], R Cavalieri[23], G Cella[14],
C Cepeda[1], E Cesarini[57], R Chakraborty[1],
T Chalermsongsak[1], S Chao[58], P Charlton[59],
E Chassande-Mottin[27], X Chen[37], Y Chen[60], A Chincarini[61],
A Chiummo[23], H S Cho[62], J Chow[63], N Christensen[64],
Q Chu[37], S S Y Chua[63], S Chung[37], G Ciani[16], F Clara[25],

D E Clark[29], J A Clark[50], F Cleva[38], E Coccia[65,66],
P-F Cohadon[46], A Colla[19,67], M Colombini[42],
M Constancio Jr[11], A Conte[19,67], R Conte[68], D Cook[25],
T R Corbitt[2], M Cordier[33], N Cornish[22], A Corsi[69],
C A Costa[11], M W Coughlin[70], J-P Coulon[38], S Countryman[28],
P Couvares[24], D M Coward[37], M Cowart[6], D C Coyne[1],
K Craig[26], J D E Creighton[12], T D Creighton[32], S G Crowder[71],
A Cumming[26], L Cunningham[26], E Cuoco[23], K Dahl[8],
T Dal Canton[8], M Damjanic[8], S L Danilishin[37], S D'Antonio[57],
K Danzmann[8,13], V Dattilo[23], B Daudert[1], H Daveloza[32],
M Davier[35], G S Davies[26], E J Daw[72], R Day[23], T Dayanga[41],
G Debreczeni[73], J Degallaix[40], E Deleeuw[16], S Deléglise[46],
W Del Pozzo[9], T Denker[8], T Dent[8], H Dereli[38], V Dergachev[1],
R De Rosa[4,52], R T DeRosa[2], R DeSalvo[68], S Dhurandhar[74],
M Díaz[32], A Dietz[17], L Di Fiore[4], A Di Lieto[14,30], I Di Palma[8],
A Di Virgilio[14], K Dmitry[34], F Donovan[10], K L Dooley[8],
S Doravari[6], M Drago[75,76], R W P Drever[77], J C Driggers[1],
Z Du[54], J-C Dumas[37], S Dwyer[25], T Eberle[8], M Edwards[7],
A Effler[2], P Ehrens[1], J Eichholz[16], S S Eikenberry[16],
G Endrőczi[73], R Essick[10], T Etzel[1], K Evans[26], M Evans[10],
T Evans[6], M Factourovich[28], V Fafone[57,66], S Fairhurst[7],
Q Fang[37], B Farr[78], W Farr[78], M Favata[79], D Fazi[78],
H Fehrmann[8], D Feldbaum[16,6], I Ferrante[14,30], F Ferrini[23],
F Fidecaro[14,30], L S Finn[80], I Fiori[23], R Fisher[24], R Flaminio[40],
E Foley[18], S Foley[10], E Forsi[6], L A Forte[4], N Fotopoulos[1],
J-D Fournier[38], S Franco[35], S Frasca[19,67], F Frasconi[14],
M Frede[8], M Frei[56], Z Frei[81], A Freise[20], R Frey[45], T T Fricke[8],
P Fritschel[10], V V Frolov[6], M-K Fujimoto[82], P Fulda[16],
M Fyffe[6], J Gair[70], L Gammaitoni[42,83], J Garcia[25], F Garufi[4,52],
N Gehrels[36], G Gemme[61], E Genin[23], A Gennai[14], L Gergely[81],
S Ghosh[41], J A Giaime[2,6], S Giampanis[12], K D Giardina[6],
A Giazotto[14], S Gil-Casanova[51], C Gill[26], J Gleason[16],
E Goetz[8], R Goetz[16], L Gondan[81], G González[2], N Gordon[26],
M L Gorodetsky[34], S Gossan[60], S Goßler[8], R Gouaty[3],
C Graef[8], P B Graff[36], M Granata[40], A Grant[26], S Gras[10],
C Gray[25], R J S Greenhalgh[84], A M Gretarsson[85], C Griffo[18],
H Grote[8], K Grover[20], S Grunewald[21], G M Guidi[43,44],
C Guido[6], K E Gushwa[1], E K Gustafson[1], R Gustafson[55],
B Hall[41], E Hall[1], D Hammer[12], G Hammond[26], M Hanke[8],
J Hanks[25], C Hanna[86], J Hanson[6], J Harms[1], G M Harry[87],
I W Harry[24], E D Harstad[45], M T Hartman[16], K Haughian[26],
K Hayama[82], J Heefner[1,125], A Heidmann[46], M Heintze[16,6],
H Heitmann[38], P Hello[35], G Hemming[23], M Hendry[26],
I S Heng[26], A W Heptonstall[1], M Heurs[8], S Hild[26], D Hoak[50],
K A Hodge[1], K Holt[6], T Hong[60], S Hooper[37], T Horrom[88],

D J Hosken[89], J Hough[26], E J Howell[37], Y Hu[26], Z Hua[54],
V Huang[58], E A Huerta[24], B Hughey[85], S Husa[51],
S H Huttner[26], M Huynh[12], T Huynh-Dinh[6], J Iafrate[2],
D R Ingram[25], R Inta[63], T Isogai[10], A Ivanov[1], B R Iyer[90],
K Izumi[25], M Jacobson[1], E James[1], H Jang[91], Y J Jang[78],
P Jaranowski[92], F Jiménez-Forteza[51], W W Johnson[2],
D Jones[25], D I Jones[93], R Jones[26], R J G Jonker[9], L Ju[37],
Haris K[94], P Kalmus[1], V Kalogera[78], S Kandhasamy[71],
G Kang[91], J B Kanner[36], M Kasprzack[23,35], R Kasturi[95],
E Katsavounidis[10], W Katzman[6], H Kaufer[13], K Kaufman[60],
K Kawabe[25], S Kawamura[82], F Kawazoe[8], F Kéfélian[38],
D Keitel[8], D B Kelley[24], W Kells[1], D G Keppel[8],
A Khalaidovski[8], F Y Khalili[34], E A Khazanov[96], B K Kim[91],
C Kim[97,91], K Kim[98], N Kim[29], W Kim[89], Y-M Kim[62], E J King[89],
P J King[1], D L Kinzel[6], J S Kissel[10], S Klimenko[16], J Kline[12],
S Koehlenbeck[8], K Kokeyama[2], V Kondrashov[1],
S Koranda[12], W Z Korth[1], I Kowalska[47], D Kozak[1],
A Kremin[71], V Kringel[8], B Krishnan[8], A Królak[99,100],
C Kucharczyk[29], S Kudla[2], G Kuehn[8], A Kumar[101],
D Nanda Kumar[16], P Kumar[24], R Kumar[26], R Kurdyumov[29],
P Kwee[10], M Landry[25], B Lantz[29], S Larson[102], P D Lasky[103],
C Lawrie[26], A Lazzarini[1], P Leaci[21], E O Lebigot[54], C-H Lee[62],
H K Lee[98], H M Lee[97], J Lee[10], J Lee[18], M Leonardi[75,76],
J R Leong[8], A Le Roux[6], N Leroy[35], N Letendre[3], B Levine[25],
J B Lewis[1], V Lhuillier[25], T G F Li[9], A C Lin[29], T B Littenberg[78],
V Litvine[1], F Liu[104], H Liu[7], Y Liu[54], Z Liu[16], D Lloyd[1],
N A Lockerbie[105], V Lockett[18], D Lodhia[20], K Loew[85],
J Logue[26], A L Lombardi[50], M Lorenzini[65], V Loriette[106],
M Lormand[6], G Losurdo[43], J Lough[24], J Luan[60],
M J Lubinski[25], H Lück[8,13], A P Lundgren[8], J Macarthur[26],
E Macdonald[7], B Machenschalk[8], M MacInnis[10],
D M Macleod[7], F Magana-Sandoval[18], M Mageswaran[1],
K Mailand[1], E Majorana[19], I Maksimovic[106], V Malvezzi[57],
N Man[38], G M Manca[8], I Mandel[20], V Mandic[71],
V Mangano[19,67], M Mantovani[14], F Marchesoni[42,107],
F Marion[3], S Márka[28], Z Márka[28], A Markosyan[29], E Maros[1],
J Marque[23], F Martelli[43,44], L Martellini[38], I W Martin[26],
R M Martin[16], D Martynov[1], J N Marx[1], K Mason[10],
A Masserot[3], T J Massinger[24], F Matichard[10], L Matone[28],
R A Matzner[108], N Mavalvala[10], G May[2], N Mazumder[94],
G Mazzolo[8], R McCarthy[25], D E McClelland[63], S C McGuire[109],
G McIntyre[1], J McIver[50], D Meacher[38], G D Meadors[55],
M Mehmet[8], J Meidam[9], T Meier[13], A Melatos[103], G Mendell[25],
R A Mercer[12], S Meshkov[1], C Messenger[26], M S Meyer[6],
H Miao[60], C Michel[40], E E Mikhailov[88], L Milano[4,52], J Miller[63],

Y Minenkov[57], C M F Mingarelli[20], S Mitra[74], V P Mitrofanov[34],
G Mitselmakher[16], R Mittleman[10], B Moe[12], M Mohan[23],
S R P Mohapatra[24,56], F Mokler[8], D Moraru[25], G Moreno[25],
N Morgado[40], T Mori[82], S R Morriss[32], K Mossavi[8], B Mours[3],
C M Mow-Lowry[8], C L Mueller[16], G Mueller[16], S Mukherjee[32],
A Mullavey[2], J Munch[89], D Murphy[28], P G Murray[26],
A Mytidis[16], M F Nagy[73], I Nardecchia[19,67], T Nash[1],
L Naticchioni[19,67], R Nayak[110], V Necula[16], I Neri[42,83],
G Newton[26], T Nguyen[63], E Nishida[82], A Nishizawa[82],
A Nitz[24], F Nocera[23], D Nolting[6], M E Normandin[32],
L K Nuttall[7], E Ochsner[12], J O'Dell[84], E Oelker[10], G H Ogin[1],
J J Oh[111], S H Oh[111], F Ohme[7], P Oppermann[8], B O'Reilly[6],
W Ortega Larcher[32], R O'Shaughnessy[12], C Osthelder[1],
C D Ott[60], D J Ottaway[89], R S Ottens[16], J Ou[58], H Overmier[6],
B J Owen[80], C Padilla[18], A Pai[94], C Palomba[19], Y Pan[49],
C Pankow[12], F Paoletti[14,23], R Paoletti[14,15], M A Papa[21,12],
H Paris[25], A Pasqualetti[23], R Passaquieti[14,30], D Passuello[14],
M Pedraza[1], P Peiris[56], S Penn[95], A Perreca[24], M Phelps[1],
M Pichot[38], M Pickenpack[8], F Piergiovanni[43,44], V Pierro[68],
L Pinard[40], B Pindor[103], I M Pinto[68], M Pitkin[26], J Poeld[8],
R Poggiani[14,30], V Poole[41], C Poux[1], V Predoi[7],
T Prestegard[71], L R Price[1], M Prijatelj[8], M Principe[68],
S Privitera[1], G A Prodi[75,76], L Prokhorov[34], O Puncken[32],
M Punturo[42], P Puppo[19], V Quetschke[32], E Quintero[1],
R Quitzow-James[45], F J Raab[25], D S Rabeling[9,48], I Rácz[73],
H Radkins[25], P Raffai[28,81], S Raja[112], G Rajalakshmi[113],
M Rakhmanov[32], C Ramet[6], P Rapagnani[19,67], V Raymond[1],
V Re[57,66], C M Reed[25], T Reed[114], T Regimbau[38], S Reid[115],
D H Reitze[1,16], F Ricci[19,67], R Riesen[6], K Riles[55],
N A Robertson[1,26], F Robinet[35], A Rocchi[57], S Roddy[6],
C Rodriguez[78], M Rodruck[25], C Roever[8], L Rolland[3],
J G Rollins[1], R Romano[4,5], G Romanov[88], J H Romie[6],
D Rosińska[31,116], S Rowan[26], A Rüdiger[8], P Ruggi[23],
K Ryan[25], F Salemi[8], L Sammut[103], V Sandberg[25],
J Sanders[55], V Sannibale[1], I Santiago-Prieto[26], E Saracco[40],
B Sassolas[40], B S Sathyaprakash[7], P R Saulson[24],
R Savage[25], R Schilling[8], R Schnabel[8,13], R M S Schofield[45],
E Schreiber[8], D Schuette[8], B Schulz[8], B F Schutz[21,7],
P Schwinberg[25], J Scott[26], S M Scott[63], F Seifert[1], D Sellers[6],
A S Sengupta[117], D Sentenac[23], A Sergeev[96], D Shaddock[63],
S Shah[118,9], M S Shahriar[78], M Shaltev[8], B Shapiro[29],
P Shawhan[49], D H Shoemaker[10], T L Sidery[20], K Siellez[38],
X Siemens[12], D Sigg[25], D Simakov[8], A Singer[1], L Singer[1],
A M Sintes[51], G R Skelton[12], B J J Slagmolen[63], J Slutsky[8],
J R Smith[18], M R Smith[1], R J E Smith[20], N D Smith-Lefebvre[1],

K Soden[12], E J Son[111], B Sorazu[26], T Souradeep[74],
L Sperandio[57,66], A Staley[28], E Steinert[25], J Steinlechner[8],
S Steinlechner[8], S Steplewski[41], D Stevens[78], A Stochino[63],
R Stone[32], K A Strain[26], S Strigin[34], A S Stroeer[32],
R Sturani[43,44], A L Stuver[6], T Z Summerscales[119],
S Susmithan[37], P J Sutton[7], B Swinkels[23], G Szeifert[81],
M Tacca[27], D Talukder[45], L Tang[32], D B Tanner[16],
S P Tarabrin[8], R Taylor[1], A P M ter Braack[9],
M P Thirugnanasambandam[1], M Thomas[6], P Thomas[25],
K A Thorne[6], K S Thorne[60], E Thrane[1], V Tiwari[16],
K V Tokmakov[105], C Tomlinson[72], A Toncelli[14,30],
M Tonelli[14,30], O Torre[14,15], C V Torres[32], C I Torrie[1,26],
F Travasso[42,83], G Traylor[6], M Tse[28], D Ugolini[120],
C S Unnikrishnan[113], H Vahlbruch[13], G Vajente[14,30],
M Vallisneri[60], J F J van den Brand[9,48], C Van Den Broeck[9],
S van der Putten[9], M V van der Sluys[78], J van Heijningen[9],
A A van Veggel[26], S Vass[1], M Vasúth[73], R Vaulin[10],
A Vecchio[20], G Vedovato[121], J Veitch[9], P J Veitch[89],
K Venkateswara[122], D Verkindt[3], S Verma[37], F Vetrano[43,44],
A Viceré[43,44], R Vincent-Finley[109], J-Y Vinet[38], S Vitale[10,9],
B Vlcek[12], T Vo[25], H Vocca[42,83], C Vorvick[25], W D Vousden[20],
D Vrinceanu[32], S P Vyachanin[34], A Wade[63], L Wade[12],
M Wade[12], S J Waldman[10], M Walker[2], L Wallace[1], Y Wan[54],
J Wang[58], M Wang[20], X Wang[54], A Wanner[8], R L Ward[63],
M Was[8], B Weaver[25], L-W Wei[38], M Weinert[8], A J Weinstein[1],
R Weiss[10], T Welborn[6], L Wen[37], P Wessels[8], M West[24],
T Westphal[8], K Wette[8], J T Whelan[56], S E Whitcomb[1,37],
D J White[72], B F Whiting[16], S Wibowo[12], K Wiesner[8],
C Wilkinson[25], L Williams[16], R Williams[1], T Williams[123],
J L Willis[124], B Willke[8,13], M Wimmer[8], L Winkelmann[8],
W Winkler[8], C C Wipf[10], H Wittel[8], G Woan[26], J Worden[25],
J Yablon[78], I Yakushin[6], H Yamamoto[1], C C Yancey[49],
H Yang[60], D Yeaton-Massey[1], S Yoshida[123], H Yum[78],
M Yvert[3], A Zadrożny[100], M Zanolin[85], J-P Zendri[121],
F Zhang[10], L Zhang[1], C Zhao[37], H Zhu[80], X J Zhu[37],
N Zotov[114,126], M E Zucker[10] and J Zweizig[1]

[1] LIGO—California Institute of Technology, Pasadena, CA 91125, USA
[2] Louisiana State University, Baton Rouge, LA 70803, USA
[3] Laboratoire d'Annecy-le-Vieux de Physique des Particules (LAPP), Université de Savoie, CNRS/IN2P3, F-74941 Annecy-le-Vieux, France
[4] INFN, Sezione di Napoli, Complesso Universitario di Monte S. Angelo, I-80126 Napoli, Italy
[5] Università di Salerno, Fisciano, I-84084 Salerno, Italy
[6] LIGO—Livingston Observatory, Livingston, LA 70754, USA
[7] Cardiff University, Cardiff, CF24 3AA, UK

[8] Albert-Einstein-Institut, Max-Planck-Institut für Gravitationsphysik, D-30167 Hannover, Germany
[9] Nikhef, Science Park, 1098 XG Amsterdam, The Netherlands
[10] LIGO—Massachusetts Institute of Technology, Cambridge, MA 02139, USA
[11] Instituto Nacional de Pesquisas Espaciais, 12227-010—São José dos Campos, SP, Brazil
[12] University of Wisconsin-Milwaukee, Milwaukee, WI 53201, USA
[13] Leibniz Universität Hannover, D-30167 Hannover, Germany
[14] INFN, Sezione di Pisa, I-56127 Pisa, Italy
[15] Università di Siena, I-53100 Siena, Italy
[16] University of Florida, Gainesville, FL 32611, USA
[17] The University of Mississippi, University, MS 38677, USA
[18] California State University Fullerton, Fullerton, CA 92831, USA
[19] INFN, Sezione di Roma, I-00185 Roma, Italy
[20] University of Birmingham, Birmingham, B15 2TT, UK
[21] Albert-Einstein-Institut, Max-Planck-Institut für Gravitationsphysik, D-14476 Golm, Germany
[22] Montana State University, Bozeman, MT 59717, USA
[23] European Gravitational Observatory (EGO), I-56021 Cascina, Pisa, Italy
[24] Syracuse University, Syracuse, NY 13244, USA
[25] LIGO—Hanford Observatory, Richland, WA 99352, USA
[26] SUPA, University of Glasgow, Glasgow, G12 8QQ, UK
[27] APC, AstroParticule et Cosmologie, Université Paris Diderot, CNRS/IN2P3, CEA/Irfu, Observatoire de Paris, Sorbonne Paris Cité, 10, rue Alice Domon et Léonie Duquet, F-75205 Paris Cedex 13, France
[28] Columbia University, New York, NY 10027, USA
[29] Stanford University, Stanford, CA 94305, USA
[30] Università di Pisa, I-56127 Pisa, Italy
[31] CAMK-PAN, 00-716 Warsaw, Poland
[32] The University of Texas at Brownsville, Brownsville, TX 78520, USA
[33] San Jose State University, San Jose, CA 95192, USA
[34] Moscow State University, Moscow, 119992, Russia
[35] LAL, Université Paris-Sud, IN2P3/CNRS, F-91898 Orsay, France
[36] NASA/Goddard Space Flight Center, Greenbelt, MD 20771, USA
[37] University of Western Australia, Crawley, WA 6009, Australia
[38] ARTEMIS, Université Nice-Sophia-Antipolis, CNRS and Observatoire de la Côte d'Azur, F-06304 Nice, France
[39] Institut de Physique de Rennes, CNRS, Université de Rennes 1, F-35042 Rennes, France
[40] Laboratoire des Matériaux Avancés (LMA), IN2P3/CNRS, Université de Lyon, F-69622 Villeurbanne, Lyon, France
[41] Washington State University, Pullman, WA 99164, USA
[42] INFN, Sezione di Perugia, I-06123 Perugia, Italy
[43] INFN, Sezione di Firenze, I-50019 Sesto Fiorentino, Firenze, Italy
[44] Università degli Studi di Urbino 'Carlo Bo', I-61029 Urbino, Italy
[45] University of Oregon, Eugene, OR 97403, USA
[46] Laboratoire Kastler Brossel, ENS, CNRS, UPMC, Université Pierre et Marie Curie, F-75005 Paris, France
[47] Astronomical Observatory Warsaw University, 00-478 Warsaw, Poland
[48] VU University Amsterdam, 1081 HV Amsterdam, The Netherlands
[49] University of Maryland, College Park, MD 20742, USA
[50] University of Massachusetts—Amherst, Amherst, MA 01003, USA
[51] Universitat de les Illes Balears, E-07122 Palma de Mallorca, Spain

[52] Università di Napoli 'Federico II', Complesso Universitario di Monte S. Angelo, I-80126 Napoli, Italy

[53] Canadian Institute for Theoretical Astrophysics, University of Toronto, Toronto, Ontario M5S 3H8, Canada

[54] Tsinghua University, Beijing 100084, People's Republic of China

[55] University of Michigan, Ann Arbor, MI 48109, USA

[56] Rochester Institute of Technology, Rochester, NY 14623, USA

[57] INFN, Sezione di Roma Tor Vergata, I-00133 Roma, Italy

[58] National Tsing Hua University, Hsinchu, Taiwan 300, Taiwan

[59] Charles Sturt University, Wagga Wagga, NSW 2678, Australia

[60] Caltech-CaRT, Pasadena, CA 91125, USA

[61] INFN, Sezione di Genova, I-16146 Genova, Italy

[62] Pusan National University, Busan 609-735, Korea

[63] Australian National University, Canberra, ACT 0200, Australia

[64] Carleton College, Northfield, MN 55057, USA

[65] INFN, Gran Sasso Science Institute, I-67100 L'Aquila, Italy

[66] Università di Roma Tor Vergata, I-00133 Roma, Italy

[67] Università di Roma 'La Sapienza', I-00185 Roma, Italy

[68] University of Sannio at Benevento, I-82100 Benevento, Italy and INFN (Sezione di Napoli), Italy

[69] The George Washington University, Washington, DC 20052, USA

[70] University of Cambridge, Cambridge, CB2 1TN, UK

[71] University of Minnesota, Minneapolis, MN 55455, USA

[72] The University of Sheffield, Sheffield S10 2TN, UK

[73] Wigner RCP, RMKI, H-1121 Budapest, Konkoly Thege Miklós út 29-33, Hungary

[74] Inter-University Centre for Astronomy and Astrophysics, Pune-411007, India

[75] INFN, Gruppo Collegato di Trento, I-38050 Povo, Trento, Italy

[76] Università di Trento, I-38050 Povo, Trento, Italy

[77] California Institute of Technology, Pasadena, CA 91125, USA

[78] Northwestern University, Evanston, IL 60208, USA

[79] Montclair State University, Montclair, NJ 07043, USA

[80] The Pennsylvania State University, University Park, PA 16802, USA

[81] MTA-Eotvos University, 'Lendulet' A. R. G., Budapest 1117, Hungary

[82] National Astronomical Observatory of Japan, Tokyo 181-8588, Japan

[83] Università di Perugia, I-06123 Perugia, Italy

[84] Rutherford Appleton Laboratory, HSIC, Chilton, Didcot, Oxon, OX11 0QX, UK

[85] Embry-Riddle Aeronautical University, Prescott, AZ 86301, USA

[86] Perimeter Institute for Theoretical Physics, Ontario, N2L 2Y5, Canada

[87] American University, Washington, DC 20016, USA

[88] College of William and Mary, Williamsburg, VA 23187, USA

[89] University of Adelaide, Adelaide, SA 5005, Australia

[90] Raman Research Institute, Bangalore, Karnataka 560080, India

[91] Korea Institute of Science and Technology Information, Daejeon 305-806, Korea

[92] Białystok University, 15-424 Białystok, Poland

[93] University of Southampton, Southampton, SO17 1BJ, UK

[94] IISER-TVM, CET Campus, Trivandrum, Kerala 695016, India

[95] Hobart and William Smith Colleges, Geneva, NY 14456, USA

[96] Institute of Applied Physics, Nizhny Novgorod, 603950, Russia

[97] Seoul National University, Seoul 151-742, Korea

[98] Hanyang University, Seoul 133-791, Korea

[99] IM-PAN, 00-956 Warsaw, Poland

[100] NCBJ, 05-400 Świerk-Otwock, Poland

[101] Institute for Plasma Research, Bhat, Gandhinagar 382428, India

[102] Utah State University, Logan, UT 84322, USA

[103] The University of Melbourne, Parkville, VIC 3010, Australia

[104] University of Brussels, B-1050 Brussels, Belgium

[105] SUPA, University of Strathclyde, Glasgow, G1 1XQ, UK

[106] ESPCI, CNRS, F-75005 Paris, France

[107] Università di Camerino, Dipartimento di Fisica, I-62032 Camerino, Italy

[108] The University of Texas at Austin, Austin, TX 78712, USA

[109] Southern University and A&M College, Baton Rouge, LA 70813, USA

[110] IISER-Kolkata, Mohanpur, West Bengal 741252, India

[111] National Institute for Mathematical Sciences, Daejeon 305-390, Korea

[112] RRCAT, Indore, MP 452013, India

[113] Tata Institute for Fundamental Research, Mumbai 400005, India

[114] Louisiana Tech University, Ruston, LA 71272, USA

[115] SUPA, University of the West of Scotland, Paisley, PA1 2BE, UK

[116] Institute of Astronomy, 65-265 Zielona Góra, Poland

[117] Indian Institute of Technology, Gandhinagar, Ahmedabad, Gujarat 382424, India

[118] Department of Astrophysics/IMAPP, Radboud University Nijmegen, PO Box 9010, 6500 GL Nijmegen, The Netherlands

[119] Andrews University, Berrien Springs, MI 49104, USA

[120] Trinity University, San Antonio, TX 78212, USA

[121] INFN, Sezione di Padova, I-35131 Padova, Italy

[122] University of Washington, Seattle, WA 98195, USA

[123] Southeastern Louisiana University, Hammond, LA 70402, USA

[124] Abilene Christian University, Abilene, TX 79699, USA

CrossMark

Abstract

In 2009–2010, the Laser Interferometer Gravitational-Wave Observatory (LIGO) operated together with international partners Virgo and GEO600 as a network to search for gravitational waves (GWs) of astrophysical origin. The sensitivity of these detectors was limited by a combination of noise sources inherent to the instrumental design and its environment, often localized in time or frequency, that couple into the GW readout. Here we review the performance of the LIGO instruments during this epoch, the work done to characterize the detectors and their data, and the effect that transient and continuous noise artefacts have on the sensitivity of LIGO to a variety of astrophysical sources.

Keywords: LIGO, gravitational waves, detector characterization

(Some figures may appear in colour only in the online journal)

[125] Deceased, April 2012.
[126] Deceased, May 2012.

1. Introduction

Between July 2009 and October 2010, the Laser Interferometer Gravitational-Wave Observatory (LIGO) [1] operated two 4 km laser interferometers as part of a global network aiming to detect and study gravitational waves (GWs) of astrophysical origin. These detectors, at LIGO Hanford Observatory, WA (LHO), and LIGO Livingston Observatory, LA (LLO)—dubbed 'H1' and 'L1', and operating beyond their initial design with greater sensitivity—took data during Science Run 6 (S6) in collaboration with GEO600 [2] and Virgo [3].

The data from each of these detectors have been searched for GW signals from a number of sources, including compact binary coalescences (CBCs) [4–6], generic short-duration GW bursts [5, 7], non-axisymmetric spinning neutron stars [8], and a stochastic GW background (SGWB) [9]. The performance of each of these analyses is measured by the searched volume of the Universe multiplied by the searched time duration; however, long and short duration artefacts in real data, such as narrow-bandwidth noise lines and transient noise events (glitches), further restrict the sensitivity of GW searches.

Searches for transient GW signals including CBCs and GW bursts are sensitive to many short-duration glitches coming from a number of environmental, mechanical, and electronic mechanisms that are not fully understood. Each search pipeline employs signal-based methods to distinguish a GW event from noise based on knowledge of the expected waveform [10–13], but also relies on careful studies of the detector behaviour to provide information that leads to improved data quality (DQ) through 'vetoes' that remove data likely to contain noise artefacts. Searches for long-duration continuous waves (CWs) and a SGWB are sensitive to disturbances from spectral lines and other sustained noise artefacts. These effects cause elevated noise at a given frequency and so impair any search over these data.

This paper describes the work done to characterize the LIGO detectors and their data during S6, and estimates the increase in sensitivity for analyses resulting from detector improvements and DQ vetoes. This work follows from previous studies of LIGO DQ during Science Run 5 (S5) [14, 15] and S6 [16, 17]. Similar studies have also been performed for the Virgo detector relating to data taking during Virgo Science Runs (VSRs) 2, 3 and 4 [18, 19].

Section 2 details the configuration of the LIGO detectors during S6, and section 3 details their performance over this period, outlining some of the problems observed and improvements seen. Section 4 describes examples of important noise sources that were identified at each site and steps taken to mitigate them. In section 5, we present the performance of data-quality vetoes when applied to each of two astrophysical data searches: the ihope CBC pipeline [13] and the Coherent WaveBurst (cWB) burst pipeline [10]. A short conclusion is given in section 6, along with plans for characterization of the next-generation Advanced LIGO (aLIGO) detectors, currently under construction.

2. Configuration of the LIGO detectors during the sixth science run

The first-generation LIGO instruments were versions of a Michelson interferometer [20] with Fabry–Perot arm cavities, with which GW amplitude is measured as a strain of the 4 km arm length, as shown in figure 1 [21]. In this layout, a diode-pumped, power-amplified Nd:YAG laser generated a carrier beam in a single longitudinal mode at 1064 nm [22]. This beam passed through an electro-optic modulator which added a pair of radio-frequency (RF) sidebands used for sensing and control of the test mass positions, before the modulated beam entered a triangular optical cavity. This cavity (the 'input mode cleaner') was configured to
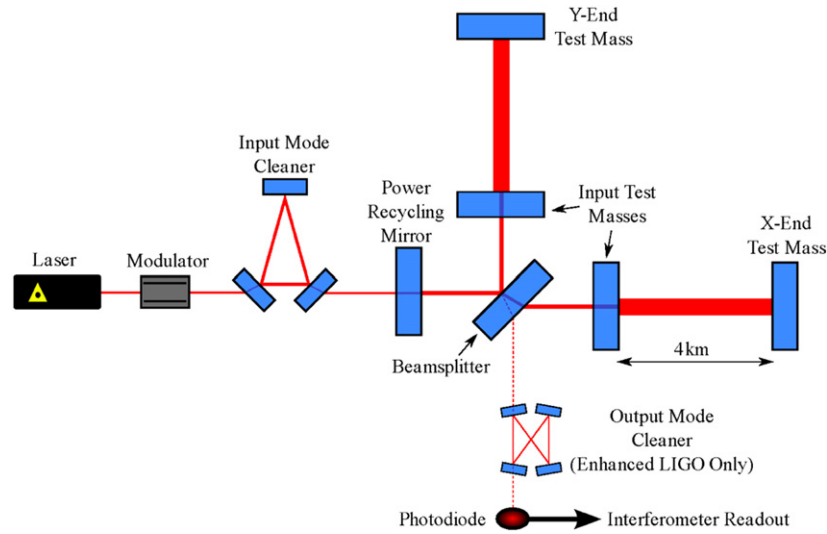
Figure 1. Optical layout of the LIGO interferometers during S6 [21]. The layout differs from that used in S5 with the addition of the output mode cleaner.

filter out residual higher-order spatial modes from the main beam before it entered the main interferometer.

The conceptual Michelson design was enhanced with the addition of input test masses at the beginning of each arm to form Fabry–Perot optical cavities. These cavities increase the storage time of light in the arms, effectively increasing the arm length. Additionally, a power-recycling mirror was added to reflect back light returned towards the input, equivalent to increasing the input laser power. During S5, the relative lengths of each arm were controlled to ensure that the light exiting each arm cavity interfered destructively at the output photo-diode, and all power was returned towards the input. In such 'dark fringe' operation, the phase modulation sidebands induced in the arms by interaction with GWs would interfere con-structively at the output, recording a GW strain in the demodulated signal. In this config-uration, the LIGO instruments achieved their design sensitivity goal over the 2 years S5 run. A thorough description of the initial design is given in [1].

For S6 a number of new systems were implemented to improve sensitivity and to prototype upgrades for the second-generation aLIGO detectors [21, 23]. The initial input laser system was upgraded from a 10 W output to a maximum of 35 W, with the installation of new master ring oscillator and power amplifier systems [24]. The higher input laser power from this system improved the sensitivity of the detectors at high frequencies (>150 Hz) and allowed prototyping of several key components for the aLIGO laser system [25]. Addition-ally, an improved CO_2-laser thermal-compensation system was installed [26, 27] to coun-teract thermal lensing caused by expansion of the test mass coating substrate due to heat from absorption of the main beam.

An alternative GW detection system was installed, replacing the initial heterodyne readout scheme [28]. A special form of homodyne detection, known as *DC readout*, was implemented, whereby the interferometer is operated slightly away from the dark fringe [29]. In this system, GW-induced phase modulations would interfere with the main beam to produce power variations on the output photodiode, without the need for demodulating the output signal. In order to improve the quality of the light incident on the output photodiode in

this new readout system, an output mode cleaner (OMC) cavity was installed to filter out the higher-order mode content of the output beam [30], including the RF sidebands. The OMC was required to be in-vacuum, but also highly stable, and so a single-stage prototype of the new aLIGO two-stage seismic isolation system was installed for the output optical platform [31], from which the OMC was suspended.

Futhermore, controls for seismic feed-forward to a hydraulic actuation system were improved at LLO to combat the higher level of seismic noise at that site [32]. This system used signals from seismometers at the Michelson vertex, and at ends of each of the arms, to suppress the effect of low-frequency ($\lesssim$10 Hz) seismic motion on the instrument.

3. Detector sensitivity during S6

The maximum sensitivity of any GW search, such as those cited in section 1, is determined by the amount of coincident multi-detector operation time and astrophysical reach of each detector. In searches for transient signals these factors determine the number of sources that could be detected during a science run, while in those for continuous signals they determine the accumulated signal power over that run.

The S6 run took place between 7 July 2009 and 20 October 2010, with each detector recording over seven months of data in that period. The data-taking was split into four epochs, A–D, identifying distinct analysis periods set by changes in detector performance or the detector network itself. Epochs A and B ran alongside the second Virgo Science Run (VSR2) before that detector was taken off-line for a major upgrade [19]. S6A ran for ~2 months before a month-long instrumental commissioning break, and S6B ran to the end of 2009 before another commissioning break. The final two epochs, C and D, spanned a continuous period of detector operation, over nine months in all, with the distinction marking the start of VSR3 and the return of a three-detector network.

Instrumental stability over these epochs was measured by the detector duty factor—the fraction of the total run time during which science-quality data was recorded. Each continuous period of operation is known as a *science segment*, defined as time when the interferometer is operating in a nominal state and the spectral sensitivity is deemed acceptable by the operator and scientists on duty. A science segment is typically ended by a critically large noise level in the instrument at which time interferometer control cannot be maintained by the electronic control system (known as *lock-loss*). However, a small number of segments are ended manually during clean data in order to perform scheduled maintenance, such as a calibration measurement. Figure 2 shows a histogram of science segment duration over the run. The majority of segments span several hours, but there are a significant number of shorter segments, symptomatic of interferometer instability. In particular, for L1 the number of shorter segments is higher than that for H1, a result of poor detector stability during the early part of the run, especially during S6B.

Table 1 summarizes the science segments for each site over the four run epochs. Both sites saw an increase in duty factor, that of H1 increasing by ~15 percentage points, and L1 by nearly 20 between epochs A and D. Additionally, the median duration of a single science-quality data segment more than doubled at both sites between the opening epochs (S6A and S6B) and the end of the run. These increases in stability highlight the developments in understanding of the critical noise couplings [1] and how they affect operation of the instruments (see section 4 for some examples), as well as improvements in the control system used to maintain cavity resonance.
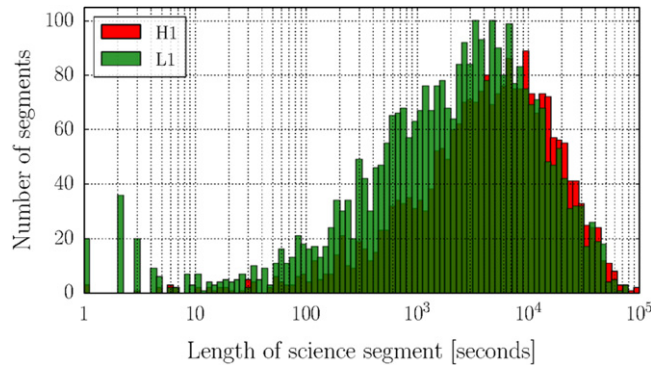
Figure 2. A histogram of the duration of each science segment for the LIGO detectors during S6. The distribution is centred around ∼1 h.
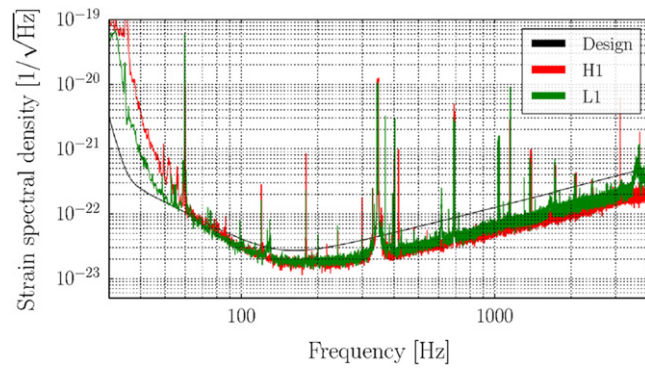

Figure 3. Typical strain amplitude sensitivity of the LIGO detectors during S6.

Table 1. Science segment statistics for the LIGO detectors over the four epochs of S6.

Epoch	Median duration (mins)	Longest duration (hours)	Total live time (days)	Duty factor (%)
(a) H1(LIGO Hanford Observatory)				
S6A	54.0	13.4	27.5	49.1
S6B	75.2	19.0	59.2	54.3
S6C	82.0	17.0	82.8	51.4
S6D	123.4	35.2	74.7	63.9
(b) L1(LIGO Livingston Observatory)				
S6A	39.3	11.8	25.6	45.7
S6B	17.3	21.3	40.0	38.0
S6C	67.5	21.4	82.3	51.1
S6D	58.2	32.6	75.2	64.3

The sensitivity to GWs of a single detector is typically measured as a strain amplitude spectral density of the calibrated detector output. This is determined by a combination of noise components, some fundamental to the design of the instruments, and some from
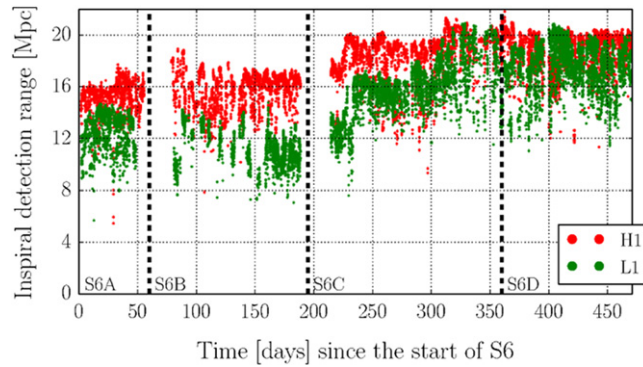
Figure 4. The inspiral detection range of the LIGO detectors throughout S6 to a binary neutron star merger, averaged over sky location and orientation. The rapid improvements between epochs can be attributed to hardware and control changes implemented during commissioning periods.

additional noise coupling from instrumental and environmental sources. Figure 3 shows the typical amplitude spectral densities of the LIGO detectors during S6. The dominant contribution below 40 Hz is noise from seismically-driven motion of the key interferometer optics, and from the servos used to control their alignment. The reduced level of the seismic wall at L1 relative to H1 can be, in part, attributed to the prototype hydraulic isolation installed at that observatory [32]. Intermediate frequencies, 50–150 Hz, have significant contributions from Brownian motion—mechanical excitations of the test masses and their suspensions due to thermal energy [33, 34]—however, some of the observed limiting noise in this band was never understood. Above 150 Hz, shot noise due to variation in incident photon flux at the output port is the dominant fundamental noise source [35]. The sensitivity is also limited at many frequencies by narrow-band line structures, described in detail in section 4.7. The spectral sensitivity gives a time-averaged view of detector performance, and so is sensitive to the long-duration noise sources and signals, but rather insensitive to transient events.

A standard measure of a detector's astrophysical reach is the distance to which that instrument could detect GW emission from the inspiral of a binary neutron star (BNS) system with a signal-to-noise ratio (SNR) of 8 [36, 37], averaged over source sky locations and orientations. Figure 4 shows the evolution of this metric over the science run, with each data point representing an average over 2048 s of data. Over the course of the run, the detection range of H1 increased from ∼16 to ∼20 Mpc, and of L1 from ∼14 to ∼20 Mpc. The instability of S6B at L1 can be seen between days 80–190, with a lower duty factor (also seen in table 1) and low detection range; this period included higher seismic noise from winter weather, although extensive commissioning of the seismic feed-forward system at LLO [32] greatly improved isolation.

The combination of increased amplitude sensitivity and improved duty factor over the course of S6 meant that the searchable volume of the Universe for an astrophysical analysis was greatly increased.

4. Data-quality problems in S6

While the previous section described the performance of the LIGO detectors over the full span of the S6 science run, there were a number of isolated problems that had detrimental

effects on the performance of each of the observatories at some time. Each of these problems, some of which are detailed below, introduced excess noise at specific times or frequencies that hindered astrophysical searches over the data.

Under ideal conditions, all excess noise sources can be quickly identified in the experimental set-up and corrected, either with a hardware change, or a modification of the control system. However, not all such fixes can be implemented immediately, or at all, and so noisy periods in auxiliary data (other data streams not directly associated with GW readout) must be noted and recorded as likely to adversely affect the GW data. During S6, these DQ flags and their associated time segments were used by analysis groups to inform decisions on which data to analyse, or which detection candidates to reject as likely noise artefacts, the impact of which will be discussed in section 5.

The remainder of this section details a representative set of specific issues that were present for some time during S6 at LHO or LLO, some of which were fixed at the source, some which were identified but could not be fixed, and one which was never identified.

4.1. Seismic noise

Throughout the first-generation LIGO experiment, the impact of seismic noise was a fundamental limit to the sensitivity to GWs below 40 Hz. However, throughout S6 (and earlier science runs), seismic noise was also observed to be strongly correlated with transient noise glitches in the detector output, not only at low frequencies, but also at much higher frequencies ($\sim 100-200$ Hz).

The top panel of figure 5 shows the seismic ground motion at LHO over a typical day. The middle panel shows transient noise events in the GW strain data as seen by the Ω-pipeline GW burst search algorithm [38, 39], while the bottom panel shows the same noise as seen by a single-interferometer CBC search. Critically, during periods of high seismic noise, the inspiral analysis 'daily ihope' [13] produced candidate event triggers across the full range of signal templates, severely limiting the sensitivity of that search.

While great efforts were made to reduce the coupling of seismic noise into the interferometer [32], additional efforts were required to improve the identification of loud transient seismic events that were likely to couple into the GW readout [40]. Such times were recorded and used by astrophysical search groups to veto candidate events from analyses, proving highly effective in reducing the noise background of such searches.

4.2. Seismically-driven length-sensing glitches

While transient seismic noise was a problem throughout the science run, during late 2009 the presence of such noise proved critically disruptive at LLO. During S6B, the majority of glitches in L1 were correlated with noise in the length control signals of two short length degrees of freedom: the power recycling cavity length (PRCL), and the short Michelson formed by the beam-splitter and the input test masses (MICH). Both of these length controls were glitching simultaneously, and these glitches were correlated with more than 70% of the glitches in the GW data.

It was discovered that high microseismic noise was driving large instabilities in the power recycling cavity that caused significant drops in the circulating power, resulting in large glitches in both the MICH and PRCL controls. These actuation signals, applied to the main interferometer optics, then coupled into the detector output.

This issue was eliminated via commissioning of a seismic feed-forward system [32] that decreased the PRC optic motion by a factor of three. The glitchy data before the fix were
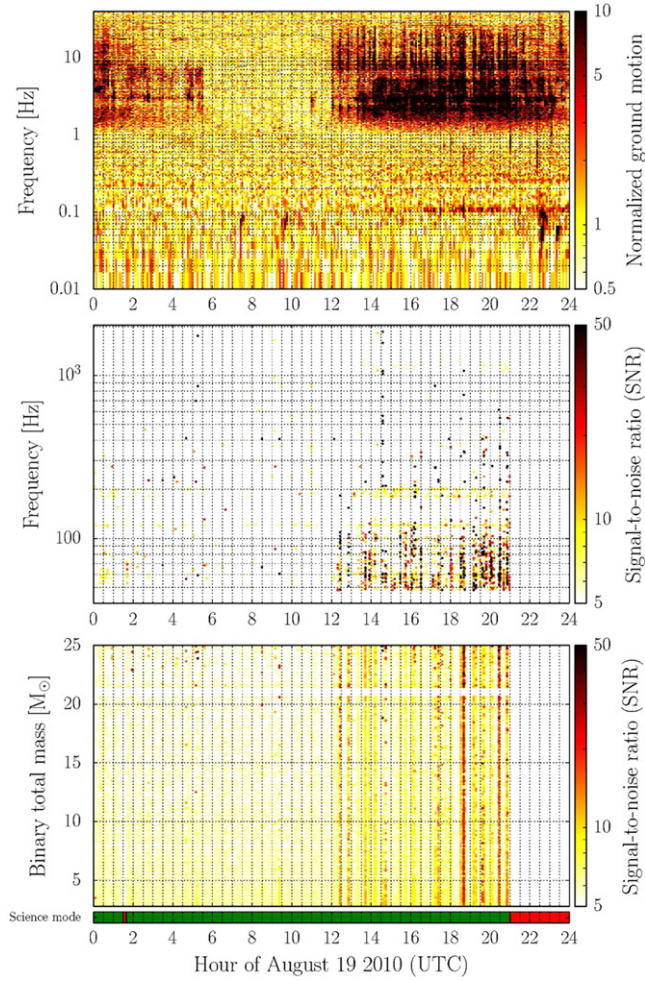
Figure 5. Seismic motion of the laboratory floor at LHO (normalized, top) and its correlation into GW burst (middle) and inspiral (bottom) analyses.

identified by both the HierarchichalVeto (HVeto) and used percentage veto (UPV) algorithms [41, 42]—used to rank auxiliary signals according to the statistical significance of glitch coincidence with the GW data—with those times used by the searches to dismiss noise artefacts from their results (more in section 5).

4.3. Upconversion of low-frequency noise due to the Barkhausen effect

In earlier science runs, as well as affecting performance below 40 Hz, increased levels of ground motion below 10 Hz had been associated with increases in noise in the 40–200 Hz band. This noise, termed seismic upconversion noise, was produced by passing trucks, distant construction activities, seasonal increases in water flow over dams, high wind, and earthquakes [15, 21, 40, 43]. During S6, this noise was often the limiting noise source at these higher frequencies. Figure 6 shows a reduction in the sensitive range to BNS inspirals, contemporaneous with the workday increase in anthropogenic seismic noise.
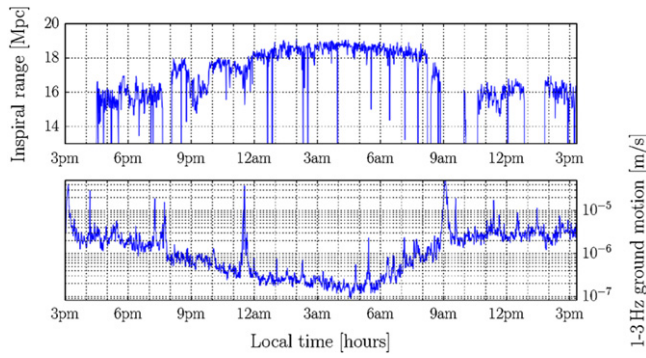
Figure 6. Sensitive distance to a binary neutron star (top) and ground motion in the 1–3 Hz band (bottom) for a day at LLO. The inverse relationship is believed to be due to nonlinear upconversion of low frequency seismic ground motions to higher frequency (∼40−200 Hz) noise in the GW output.
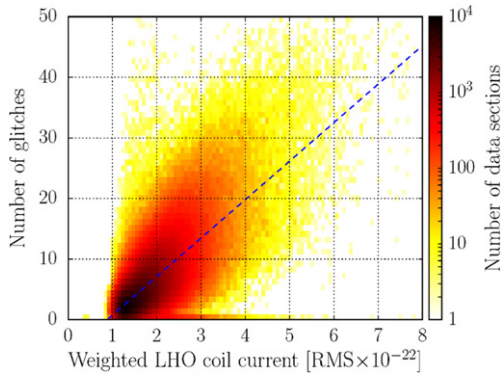

Figure 7. Correlation between low SNR glitches in the GW data, and current in the test mass coil at H1. This correlation is indicative of the Barkhausen effect.

Experiments subsequently showed that seismic upconversion noise levels correlated better with the amplitudes of the currents to the electromagnets that held the test masses in place as the ground moved than with the actual motion of the test masses or of the ground. An empirical, frequency-dependent function was developed to estimate upconversion noise from the low-frequency test mass actuation currents. This function was used to produce flags that indicated time periods that were expected to have high levels of seismic upconversion noise.

In addition to average reductions in sensitivity, upconverted seismic noise transients further reduced sensitivity to unmodelled GW bursts. Figure 7 shows that the rate of low-SNR glitches in the GW data—in a frequency band above that expected from linear seismic noise coupling—was correlated with the test mass actuation current, suggesting that seismic upconversion was the source of a low-SNR noise background that limited GW burst detection.

Investigations found that seismic upconversion noise bursts were clustered in periods of high slope in the amplitude of the magnetic actuator current. This was evidence that the seismic upconversion noise was Barkhausen noise [44]: magnetic field fluctuations produced by avalanches of magnetic domains in ferromagnetic materials that occur when the domains

align with changing magnetic fields. The Barkhausen noise hypothesis was supported by investigations in which the noise spectrum was reproduced by magnetic fields that were generated independently of the system.

These investigations also suggested that the putative source of the Barkhausen noise was near or inside the test mass actuators. It was originally thought that the source of this upconversion noise was Barkhausen noise from NbFeB magnets, but a swap to less noisy SmCo magnets did not significantly reduce the noise [45]. However, it was found that fasteners inside the magnetic actuator, made of grade 303 steel, were ferromagnetic, probably because they were shaped or cut when cold. For aLIGO, grade 316 steel, which is much less ferromagnetic after cold working, is being used at the most sensitive locations.

4.4. Beam jitter noise

As described previously, one of the upgrades installed prior to S6 was the OMC, a bow-tie-shaped cavity designed to filter out higher-order modes of the main laser beam before detection at the output photodiode. As known from previous experiments at GEO600 [46], the mode transmission of this cavity is very sensitive to angular fluctuations of the incident beam, whereby misalignment of the beam would cause nonlinear power fluctuations of the trans-mitted light [29, 47].

At LIGO, low-frequency seismic noise and vibrations of optical tables were observed to mix with higher-frequency beam motion (jitter) on the OMC to produce noise sidebands around the main jitter frequency. The amplitude of these sidebands was unstable, changing with the amount of alignment offset, resulting in transient noise at these frequencies, the most sensitive region of the LIGO spectrum, as seen in figure 5 (middle panel). Mitigation of these glitches involved modifications of the suspension system for the auxiliary optics steering the beam into the OMC, to minimize the coupling of optical table motion to beam motion. Additionally, several other methods were used to mitigate and control beam jitter noise throughout the run: full details are given in [29].

4.5. Mechanical glitching at the reflected port

While the problems described up to this point have been inherent to the design or construction of either interferometer, the following two issues were both caused by electronics failures associated with the LHO interferometer.

The first of these was produced by faults in the servo actuators used to stabilize the pointing of the beam at the reflected port of the interferometer. This position is used to sense light reflected from the PRC towards the input, and generate control signals to correct for arm-cavity motion. The resulting glitches coupled strongly into the GW data at ~37 Hz and harmonics.

The source of the glitches was identified with the help of HVeto, which discovered that a number of angular and length sensing channels derived from photodiodes at the reflected port were strongly coupled with events in the GW data. Figure 8 shows the broad peaks in the spectra of one length sensing channel and the un-calibrated GW readout compared to a quiet reference time. On top of this, accelerometer signals from the optical table at the reflected port were found to be coupling strongly, having weak but coincident glitches.

These accelerometer coincidences indicated that the glitches were likely produced by mechanical motions of steering mirrors resulting from a faulty piezoelectric actuation system. Because of this, this servo was decommissioned for the rest of the run, leading to an overall improvement in DQ.
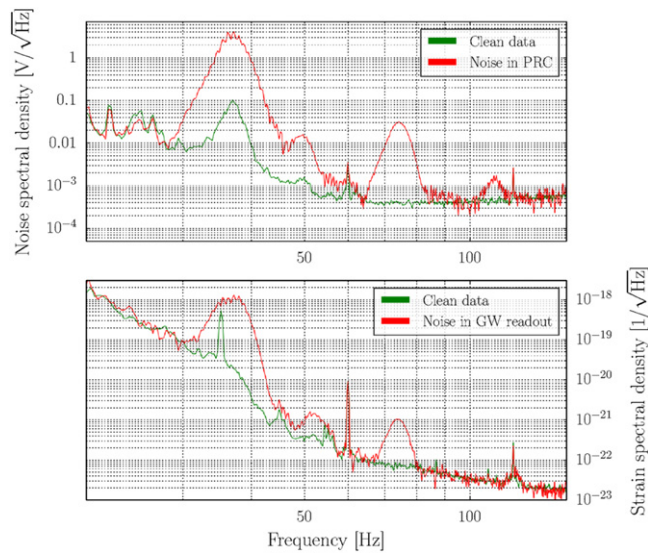
Figure 8. Broad noise peaks centred at 37 Hz and its harmonics in the power recycling cavity length signal (top) and the GW output error signal (bottom). Each panel shows the spectrum as a noisy period (red) in comparison with a reference taken from clean data (green).
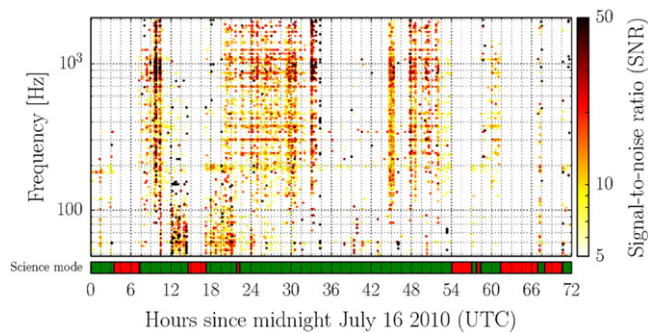

Figure 9. Noise events in the GW strain data recorded by the Ω-pipeline over a 60 h period at LHO. The high SNR events above 100 Hz in hours 7–10, 20–34, and 44–42, were caused by broadband noise from a faulty electrical connection. The grid-like nature of these events is due to the discrete tiling in frequency by the trigger generator.

4.6. Broadband noise bursts from poor electrical connections

The second of the electronics problems caused repeated, broadband glitching in the LHO GW readout towards the end of S6. Periods of glitching would last from minutes to hours, and greatly reduced the instrumental sensitivity over a large frequency range, as shown in figure 9.

The main diagnostic clues were coincident, but louder, glitches in a set of quadrant photo-diodes (QPDs) sensing beam motion in the OMC. It was unlikely that these sensors could detect a glitch in the beam more sensitively than the GW readout photo-diode, and so the prime suspect then became the electronics involved with recording data from these QPDs.
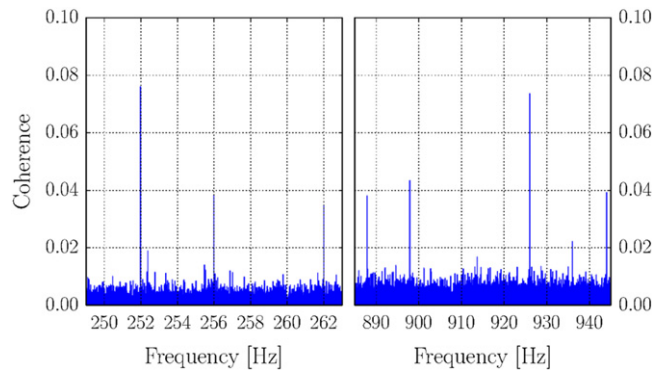
Figure 10. The coherence between the L1 GW readout signal and data from a magnetometer in the central building at LLO over one week of March 2010. 2 and 16 Hz harmonics were seen to be coherent at numerous locations across the operating band of both interferometers, affecting the sensitivity of long-duration GW searches.

In the process of isolating the cause, several other electronics boards in the OMC were inspected, re-soldered, and swapped for spares. The problem was finally solved by re-soldering the connections on the electronics board that provided the high-voltage power supply to drive a piezoelectric transducer.

4.7. Spectral lines

Just as searches for transient signals are limited by instrumental glitches, so too our searches for steady signals are limited by a number of instrumental narrow-band peaks representing specific frequencies at which noise was elevated for a significant amount of time, in many cases for the entire science run. Many spectral lines are fundamental to the design and operation of the observatories, including alternating current power lines from the US mains supply, at 60 Hz; violin modes from core-optic suspensions, around 350 Hz; and various calibration lines used to measure the interferometer response function.

Each of these features can be seen in figure 3 at their fundamental frequency and a number of harmonics; however, also seen are a large number of lines from unintended sources, such as magnetic and vibrational couplings. These noise lines can have a damaging effect on any search for GWs if the frequencies of the incoming signal and of the lines overlap for any time; this is especially troublesome for searches for continuous GW emitters.

Throughout S6, series of lines were seen at both observatories as 2 and 16 Hz harmonics. Figure 10 shows two separate groups of peaks in these harmonic sets found in coherence between the GW data for L1 and a magnetometer located near the output photo-detector. These lines were a serious concern for both the CW and SGWB searches due to their appearance at both observatories [48], leading to contamination of the coincidence-based searches for CW sources. Investigations indicated that the 2 Hz comb was likely related to problems with the data acquisition system. However, the mechanism was never fully identified, and the lines persisted throughout most of the run.

A number of other lines were isolated at either observatory site [48], and while not discussed in detail here, the cumulative effect of all spectral lines on searches for long-duration GW sources is discussed in detail in section 5.
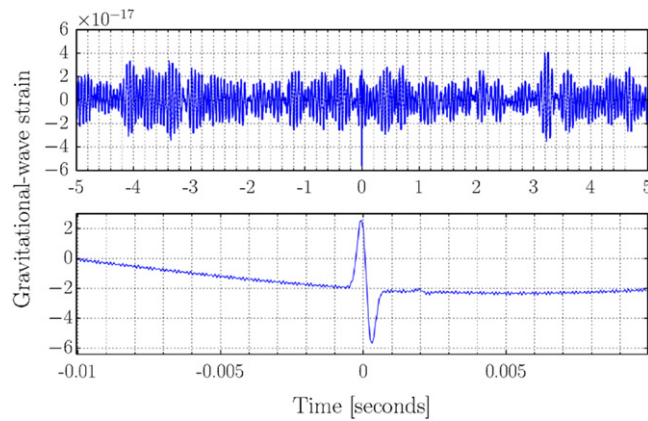
Figure 11. A spike glitch in the raw GW photodiode signal for L1. The top panel shows the glitch in context with 10 s of data, while the bottom shows the glitch profile as described in the text.

4.8. The 'spike' glitch

The spike glitch was the name given to a class of very loud transients seen in the L1 instrument. They were characterized by a distinctive shape in the time series of the signal on the GW output photodiode, beginning with a rapid but smooth dip (lasting ∼1 ms) before a period of damped oscillation lasting ∼3 milliseconds, as shown in figure 11. The amplitude of these glitches was extremely large, often visible in the raw time-series (which is normally dominated by low-frequency seismic motion), with the Ω-pipeline typically resolving these events with SNRs ranging from 200 to well over 20 000.

The size and rapidity of the initial glitch suggested that the source was after the beams had re-combined at the beam-splitter before detection at the readout photodiode. The damped oscillations after the initial dip, however, were likely due to the response of the length control loop of the interferometer, meaning an actual or apparent sudden dip in the light on the output photodiode could explain the entire shape of the spike glitch. To investigate this possibility, the interferometer was run in a configuration where the light did not enter the arm cavities, but went almost directly into the OMC, removing the length and angular control servos from consideration. Sharp downward dips in the light were seen during this test, although they were 0.2 milliseconds wide, much narrower than the initial dips of the spike glitches.

Despite this investigation and many others, the cause of the spike glitch was never determined. However, these glitches were clearly not of astrophysical origin, and were not coherent with similar events in H1, allowing the CBC signal search to excise them from analyses by vetoing time around glitches detected in L1 with unreasonably high SNR. For future science runs, aLIGO will consist of almost entirely new hardware, so whether the spike glitch or something very similar will be seen in new data remains to be seen.

5. The impact of DQ on GW searches

The impact of non-Gaussian, non-stationary noise in the LIGO detectors on searches for GWs is significant. Loud glitches, such as the spike glitch, can mask or greatly disrupt transient GW signals present in the data at the same time, while high rates of lower SNR glitches can significantly increase the background in searches for these sources. Additionally, spectral

lines and continued glitching in a given frequency range reduces the sensitivity of searches for long-duration signals at those frequencies. Both long- and short-duration noise sources have a notable effect on astrophysical sensitivity if not mitigated.

Non-Gaussian noise in the detector outputs that can be correlated with auxiliary signals that have negligible sensitivity to GWs can be used to create flags for noisy data; these flags can then be used in astrophysical searches to remove artefacts and improve sensitivity. With transient noise, the flags are used to identify time segments in which the data may contain glitches.

5.1. DQ vetoes for transient searches

In this section, the impact of noisy data is measured by its effect on the primary analyses of the LIGO–Virgo transient search groups [4, 7]:

- the low-mass CBC search 'ihope' [13] is a coincidence-based analysis in which data from each detector are filtered against a bank of binary inspiral template signals, producing an SNR time-series for each. Peaks in SNR across multiple detectors are considered coincident if the separation in time and matched template masses are small [49]. This analysis also uses a χ^2-statistic test to down-rank signals with high SNR but a spectral shape significantly different to that of the matched template [50].
- The all-sky cWB algorithm [10] calculates a multi-detector statistic by clustering time-frequency pixels with significant energy that are coherent across the detector network.

In both cases, the multi-detector events identified are then subject to a number of consistency tests before being considered detection candidates.

The background of each search is determined by relatively shifting the data from multiple detectors in time. These time shifts are much greater than the time taken for a GW to travel between sites, ensuring that any multi-detector events in these data cannot have been produced by a single astrophysical signal.

Although both searches require signal power in at least two detectors, strong glitches in a single detector coupled with Gaussian noise in others still contributed significantly to the search background during S6. Data quality (DQ) flags were highly effective in removing these noise artefacts from the analyses. The effect of a time-domain DQ flag can be described by its *deadtime*, the fraction of analysis time that has been vetoed; and its *efficiency*, the fractional number of GW candidate events removed by a veto in the corresponding deadtime.

Flag performances are determined by their efficiency-to-deadtime ratio (EDR); random flagging and vetoing of data gives EDR $\simeq 1$, whereas effective removal of glitches gives a much higher value. Additionally, the *used percentage*—the fraction of auxiliary channel glitches which coincide with a GW candidate event—allows a measure of the strength of the correlation between the auxiliary and GW channel data.

Each search group chose to apply a unique set of DQ flags in order to minimize deadtime while maximizing search sensitivity; for example, the CBC search teams did not use a number of flags correlated with very short, high-frequency disturbances, as these do not trigger their search algorithm, while these flags were used in searches for unmodelled GW bursts.

We present the effect of three categories of veto on each of the above searches in terms of reduction in analysable time and removal of noise artefacts from the search backgrounds. Only brief category definitions are given, for full descriptions see [15].

Table 2. Summary of the reduction in all time and analysable time by category 1 veto segments during S6.

Instrument	Absolute deadtime % (seconds)		Search deadtime % (seconds)	
	cWB	ihope	cWB	ihope
H1	0.3% (53318)	0.4% (176079)	0.4% (77617)	3.8% (786284)
L1	0.4% (75016)	0.1% (20915)	0.7% (137115)	6.2% (1180976)

5.1.1. Category 1 vetoes. The most egregious interferometer performance problems are flagged as category 1. These flags denote times during data taking when the instrument was not running under the designed configuration, and so should not be included in any analysis.

The data monitoring tool (DMT) automatically identified certain problems in real time, including losses of cavity resonance, and errors in the $h(t)$ calibration. Additionally, scientists monitoring detector operation in the control room at each observatory manually flagged individual time segments that contained observed instrumental issues and errors.

All LIGO-Virgo search groups used category 1 vetoes to omit unusable segments of data; as a result their primary effect was in the reduction in analysable time over which searches were performed. This impact is magnified by search requirements on the duration for analysed segments, with the cWB and ihope searches requiring a minimum of 316 and 2064 s of contiguous data respectively. Table 2 outlines the absolute deadtime (fraction of science-quality data removed) and the search deadtime (fractional reduction in analysable time after category 1 vetoes and segment selection). At both sites the amount of science-quality time flagged as category 1 is less than half of one percent, highlighting the stability of the instrument and its calibration. However, the deadtime introduced by segment selection is significantly higher, especially for the CBC analysis. The long segment duration requirement imposed by the ihope pipeline results in an order of magnitude increase in search deadtime relative to absolute deadtime.

5.1.2. Categories 2 and 3. The higher category flags were used to identify likely noise artefacts. Category 2 veto segments were generated from auxiliary data whose correlation with the GW readout has been firmly demonstrated by instrumental commissioning and investigations. Category 3 includes veto segments from less well understood statistical correlations between noisy data in an auxiliary channel and the GW readout. Both the ihope and cWB search pipelines produce a first set of candidate event triggers after application of category 2 vetoes, and a reduced set after application of category 3.

The majority of category 2 veto segments were generated in low-latency by the DMT and include things like photodiode saturations, digital overflows, and high seismic and other environmental noise. At category 3, the HVeto [41], UPV [42], and bilinear-coupling veto [51] algorithms were used, by the burst and CBC analyses respectively, to identify coupling between auxiliary data and the GW readout.

Table 3 gives the absolute, relative, and cumulative deadtimes of these categories after applying category 1 vetoes and segment selection criteria, outlining the amount of analysed time during which event triggers were removed. As with category 1, category 2 vetoes have deadtime $\mathcal{O}(1)\%$, but with significantly higher application at L1 compared to H1. This is largely due to one flag used to veto the final 30 s before any lock loss, due to observed instrumental instability, combined with the relative abundance of short data-taking segments
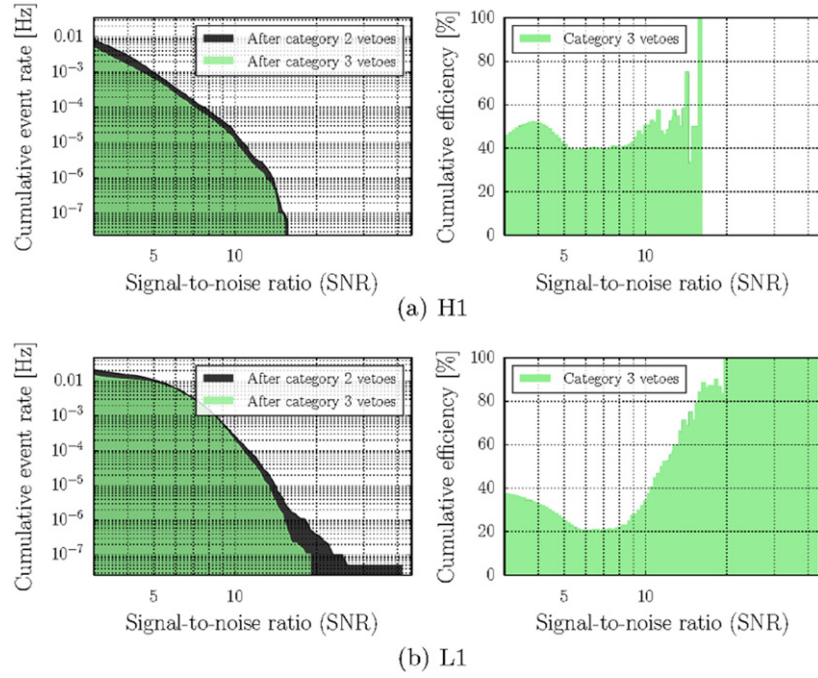
Figure 12. The effect of category 3 vetoes on the cWB pipeline for (a) H1 and (b) L1. The left panels show the reduction in event rate, while the right panels show the cumulative veto efficiency, both as a function of single-detector SNR.

for L1. Additionally, photodiode saturations and computational timing errors were more prevalent at the LLO site than at LHO and so contribute to higher relative deadtime.

Category 3 flags contributed $\mathcal{O}(10)\%$ deadtime for each instrument. While this level of deadtime is relatively high, as we shall see, the efficiency of these flags in removing background noise events makes such cuts acceptable to the search groups.

Figure 12 shows the effect of category 3 vetoes on the background events from the cWB pipeline; these events were identified in the background from time time-slides and are plotted using the SNR reconstructed at each detector. This search applies category 2 vetoes in memory, and does not record any events before this step, so efficiency statements are only available for category 3. The results are shown after the application of a number of network- and signal-consistency checks internal to the pipeline that reject a large number of the loud events. As a result, the background is dominated by low SNR events, with a small number of loud outliers. At both sites, DQ vetoes applied to this search have cumulative EDR ⩾5 at SNR 3, with those at L1 removing the tail above SNR 20. However, despite the reduction, this search was still severely limited by the remaining tail in the multi-detector background distribution [7].

Figure 13 shows the effect of category 2 and 3 vetoes on the background from the CBC ihope pipeline; this search sees a background extending to higher SNR. As shown, the background is highly suppressed by DQ vetoes, with an efficiency of 50% above SNR 8, and 80% above ∼100 at both sites. The re-weighted SNR statistic, as defined in [13], is highly effective in down-ranking the majority of outliers with high matched-filter SNR, but a non-Gaussian tail was still present at both sites. Category 3 vetoes successfully removed this tail,

Table 3. Summary of the absolute, relative, and cumulative deadtimes introduced by category 2 and 3 veto segments during S6. The relative deadtime is the additional time removed by category 3 not vetoed by category 2, and cumulative deadtime gives the total time removed from the analysis.

Deadtime type	Cat.	H1		L1	
		cWB	ihope	cWB	ihope
Absolute % (s)	2	0.26%	0.77%	1.59%	1.53%
	3	7.90%	9.26%	8.54%	7.03%
Relative % (s)	3	7.73%	9.00%	7.06%	6.10%
Cumulative % (s)	3	7.97%	9.71%	8.54%	7.54%
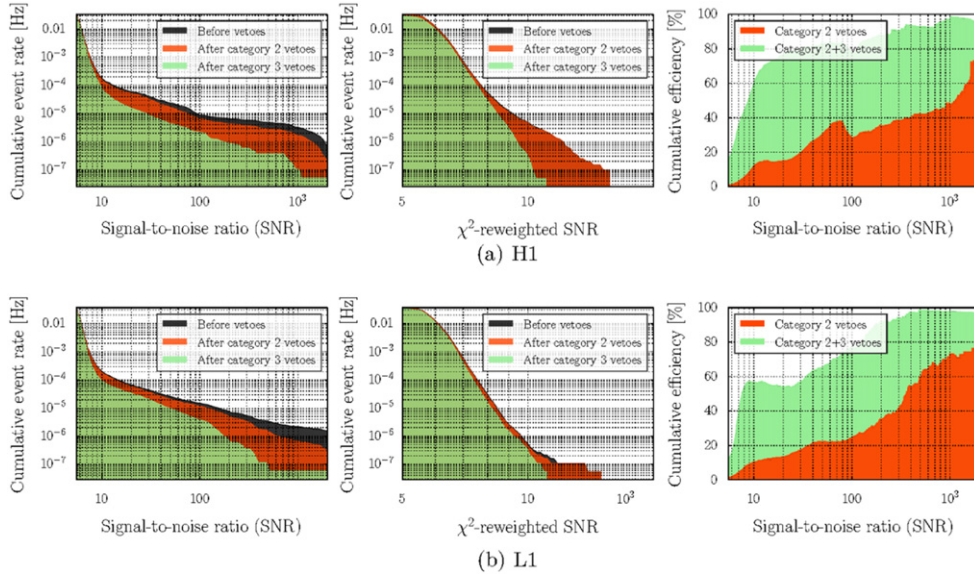
Figure 13. The effect of category 2 and jointly of category 2 and 3 vetoes on the CBC ihope pipeline for (a) H1 and (b) L1. The left panels show the reduction in event rate as a function of SNR, the centre panels show the reduction in event rate as a function of the χ^2-weighted SNR, and the right panels show the cumulative efficiency as a function of SNR.

reducing the loudest event at H1 (L1) from a re-weighted SNR of 16.0 (15.3) to 11.1 (11.2). Search sensitive distance was roughly inversely proportional to the χ^2-weighted SNR of the loudest event, and so reducing the loudest event by $\sim$30% with $\sim$10% deadtime can be estimated as a factor of $\sim$2.5 increase in detectable event rate.

5.2. DQ in searches for long-duration signals

In searches for both continuous GWs and a SGWB, the duration and stationarity of data from each detector were the key factors in search sensitivity. These analyses integrate over the entire science run in order to maximize the SNR of a low-amplitude source. Accordingly, they

were impacted only very little by infrequent glitches, but were adversely affected by spectral lines and long periods of glitching in a given frequency band.

5.2.1. Searches for continuous GWs. The PowerFlux pipeline [52, 53] is one method used to conduct an all-sky search for GW signals from pulsars. This search, currently in progress, has chosen the final seven months of the S6 dataset in order to minimize the impact of poor detector performance from the earlier epochs.

A preliminary analysis of the data has shown instrumental features at high frequency causing the search sensitivity to drop towards that observed during S5. In all, ~20% of frequency bands, each a few hundred mHz wide, have been identified as non-Gaussian, compared to almost zero in S5. This increase can be attributed to problems with the data acquisition system, which is thought to have produced the comb of 2 Hz lines described in section 4.7, and increased sensitivity to beam jitter introduced by the OMC along with the new DC readout scheme (section 4.4).

5.2.2. Searches for a SGWB. For the S6 search for a SGWB, DQ cuts were made to eliminate data in H1 and L1 that were too noisy, too non-stationary, or that had apparent correlated noise between detectors[127]. The analyses ran over times when both LIGO detectors were taking science-quality data, excluding times flagged as category 1 and those including hardware injections [54]. The category 1 segments chosen for this search caused a 2% reduction in coincident data for the LIGO detector pair.

In addition, up to 5.5% of data segments deviate from the stationary noise assumption, depending on frequency. These were removed from the analysis by identifying segments whose standard deviation, σ, varies from neighbouring segments by greater than 20%. After applying all of the DQ cuts, ~117 days of coincident live time for the LIGO network remained.

Spectral noise lines are also a problem for the SGWB search. It is improbable to have a spectral noise line present in the same frequency bin (0.25 Hz) in both H1 and L1, but it is possible. In addition, a loud line in one detector can couple with a noise fluctuation in the other and produce an excess when the correlation is calculated between the two data streams. In order to examine frequency bins for contamination, the coherence between two interferometers was calculated,

$$\Gamma(f) = \frac{|\langle P_{12}(f)\rangle|^2}{\langle P_1(f)\rangle\langle P_2(f)\rangle}, \tag{1}$$

where $\langle P_{12}(f)\rangle$ is the average cross-spectral density and $\langle P_i(f)\rangle$ is the power spectral density for the ith interferometer. This was used to identify high coherence bins, searching at resolutions of 1 Hz and 100 mHz, using the method in [9]. This identified power line harmonics, 16 Hz harmonics from data acquisition, violin modes of the interferometer mirror suspension, and injected calibration signals. These frequencies were excluded from the analysis, as were some frequency bins where a clear association with an environmentally produced noise line in either the H1 or L1 data could be made. In total, 87 frequency bins (each 0.25 Hz wide, in the range from 40–1000 Hz) were removed from the S6 LIGO SGWB search. The study of the coherence also revealed a small amount (0.2%) of additional non-stationary time series data, and these were excluded.

---

[127] In the absence of a signal model, correlated noise and a GW signal are indistinguishable in a stochastic search. However, a stochastic isotropic search assumes that the signal is broadband, and so narrow-band line features can be considered to be of instrumental, usually electronic, origin.

In addition, the SGWB search pipeline was run over LIGO data after a non-physical time-shift had been applied. The inspection of these data revealed further frequency bins where the SNR was greater than 4.25. If frequency bins met this condition for at least two of the time shifted runs, they were removed from the final foreground analysis. This removed seven more frequency bins.

Preliminary results from the S6 CW and SGWB searches indicate that these steps have cleaned the data set, allowing more sensitive searches. However, the increased non-stationarity and noise lines during S6 relative to S5 have produced a further detrimental effect on the data. The S6 CW searches can be expected to set better upper limits on GW amplitudes than the S5 searches, nevertheless, spectral lines will appear as potential sources for all-sky CW signal searches, and much work remains to explain the source of these presumed noise lines. On the SGWB side, the S6 data will provide a better upper limit as compared to the S5 results [9, 55].

It should also be noted that correlated magnetic field noise, from the Schumann resonances, was observed in correlations between magnetometers at H1, L1 and Virgo. However it was determined that the level of correlated noise did not effect the S5 or S6 stochastic searches [56].

6. Conclusions and outlook for aLIGO

The LIGO instruments, at both Hanford and Livingston, are regularly affected by both non-Gaussian noise transients and long-duration spectral features. Throughout S6 a number of problems were identified as detrimental to stable and sensitive data-taking at the observatories, as well as to the astrophysical searches performed on the data.

Instrumental fixes employed throughout the science run resulted in increasingly stable and sensitive instruments. Median segment duration and overall duty factor improved from epoch to epoch (table 1) and the detection range to the canonical BNS inspiral increased by a significant factor (figure 4). DQ flags, used to identify known correlations between noise in auxiliary systems and the GW data, figures allowed for a significant reduction in the event background of both core transient searches, ihope and cWB (figures 12, 13). An EDR above 5 for both searches, at both sites, allowed for a significant increase in the sensitivity of the search, improving the upper limits on event rate for both CBC and generic GW burst sources.

However, a tail of high SNR events was still present in the cWB search for GW bursts, requiring deeper study of the glitch morphology and improved identification methods. Additionally, the presence of noise lines outside the instrumental design had a detrimental, but not debilitating, effect on searches for long-duration signals. A large number of these remaining transient and long-duration noise sources are still undiagnosed, meaning a large effort must be undertaken to mitigate similar effects in the second-generation instruments.

The first-generation LIGO instruments were decommissioned shortly following the end of the science run (although immediately after S6 shot noise reduction was demonstrated in the H1 interferometer by using squeezed states of light [57]), and installation and early testing of aLIGO systems is now under way [23]. With the next data-taking run scheduled for 2015 [58], many methods and tools developed during the last run are set to be upgraded to further improve instrument and DQ. Improvements are in place for each of the noise event detection algorithms, allowing for more accurate detection of transient noise in all channels, and work is ongoing for the HVeto and Used Percentage Veto (UPV) statistical veto generators [59] to enable more efficient identification of sources of noise in the GW data. In addition, multivariate statistical classifiers are being developed for use in glitch identification [60], using

more information produced from event triggers to improve veto efficiency and identification of false alarms with minimal deadtime.

One of the major goals of the aLIGO project is to contribute to multi-messenger astronomy—the collaboration between GW observatories and electromagnetic (EM) and neutrino observatories [61, 62]. Both the burst and CBC search working groups are developing low-latency analyses from which to trigger followup with partner EM telescopes, requiring a much greater effort in low-latency characterization of the data. With this in mind, a large part of the development in detector characterization in the LIGO Scientific Collaboration is now being devoted to real-time characterization of instrumental data, including the GW output and all auxiliary channels. An online detector characterization system is being developed for aLIGO that summarizes the status of all instrumental and environmental systems in real-time to allow fast identification of false alarms in these on-line analyses, and reduce the latency of EM follow-up requests.

Best estimates predict ∼40 detections of GWs from BNS mergers per year at design sensitivity [63], assuming stationary, Gaussian noise. A great effort will be required in commissioning the new instruments to achieve these goals, including detailed characterization of their performance before the start of the first advanced observing run.

Acknowledgments

References

[1] Abbott B P *et al* 2009 LIGO: the Laser Interferometer Gravitational-Wave Observatory *Rep. Prog. Phys.* **72** 076901
[2] Grote H 2008 The status of GEO 600 *Class. Quantum Grav.* **25** 114043
[3] Acernese F *et al* 2008 Status of Virgo *Class. Quantum Grav.* **25** 114045
[4] Abadie J *et al* 2012 Search for gravitational waves from low mass compact binary coalescence in LIGO's sixth science run and Virgo's science runs 2 and 3 *Phys. Rev.* D **85** 082002

[5] Abadie J *et al* 2012 Search for gravitational waves associated with gamma-ray bursts during LIGO science run 6 and Virgo science runs 2 and 3 *Astrophys. J.* **760** 12

[6] Aasi J *et al* 2013 Search for gravitational waves from binary black hole inspiral, merger, and ringdown in LIGO–Virgo data from 2009–2010 *Phys. Rev.* D **87** 022002

[7] Abadie J *et al* 2012 All-sky search for gravitational-wave bursts in the second joint LIGO–Virgo run *Phys. Rev.* D **85** 122007

[8] Aasi J *et al* 2013 Einstein@Home all-sky search for periodic gravitational waves in LIGO S5 data *Phys. Rev.* D **87** 042001

[9] Abbott B P *et al* 2009 An upper limit on the stochastic gravitational-wave background of cosmological origin *Nature* **460** 990

[10] Klimenko S, Yakushin I, Mercer R A and Mitselmakher G 2008 A coherent method for detection of gravitational wave bursts *Class. Quantum Grav.* **25** 114029

[11] Sutton P J *et al* 2010 X-pipeline: an analysis package for autonomous gravitational-wave burst searches *New J. Phys.* **12** 053034

[12] Harry I W and Fairhurst S 2011 A targeted coherent search for gravitational waves from compact binary coalescences *Phys. Rev.* D **83** 084002

[13] Babak S *et al* 2013 Searching for gravitational waves from binary coalescence *Phys. Rev.* D **87** 24033

[14] Blackburn L *et al* 2008 The LSC glitch group: monitoring noise transients during the fifth LIGO science run *Class. Quantum Grav.* **25** 184004

[15] Slutsky J *et al* 2010 Methods for reducing false alarms in searches for compact binary coalescences in LIGO data *Class. Quantum Grav.* **27** 165023

[16] Christensen N 2010 LIGO S6 detector characterization studies *Class. Quantum Grav.* **27** 194010

[17] McIver J 2012 Data quality studies of enhanced interferometric gravitational wave detectors *Class. Quantum Grav.* **29** 124010

[18] Robinet F 2010 The LIGO Scientific Collaboration and the Virgo Collaboration data quality in gravitational wave bursts and inspiral searches in the second Virgo science run *Class. Quantum Grav.* **27** 194012

[19] Aasi J *et al* 2012 The characterization of Virgo data and its impact on gravitational-wave searches *Class. Quantum Grav.* **29** 155002

[20] Michelson A A and Morley E W 1887 On the relative motion of the Earth and of the luminiferous ether *Sidereal Messenger* **6** 306–10

[21] Smith J R 2009 The path to the enhanced and advanced LIGO gravitational-wave detectors *Class. Quantum Grav.* **26** 114013

[22] Savage R L, King P J and Seel S U 1998 A highly stabilized 10 Watt Nd:YAG laser for the Laser Interferometer Gravitational-Wave Observatory (LIGO) *Laser Phys.* **8** 679–85

[23] Harry G M 2010 Advanced LIGO: the next generation of gravitational wave detectors *Class. Quantum Grav.* **27** 084006

[24] Adhikari R, Fritschel P and Waldman S J 2006 Enhanced LIGO *Technical Report* LIGO-T060156 LIGO Laboratory

[25] Kwee P *et al* 2012 Stabilized high-power laser system for the gravitational wave detector advanced LIGO *Opt. Express* **20** 10617–34

[26] Ballmer S *et al* 2005 Thermal compensation system description *Technical Report* T050064

[27] Amin R S and Giaime J A 2010 Gravitational-wave detector-derived error signals for the LIGO thermal compensation system *Class. Quantum Grav.* **27** 215002

[28] Fritschel P, Bork R, González G, Mavalvala N, Ouimette D, Rong H, Sigg D and Zucker M 2001 Readout and control of a power-recycled interferometric gravitational-wave antenna *Appl. Opt.* **40** 4988–98

[29] Fricke T T *et al* 2012 DC readout experiment in Enhanced LIGO *Class. Quantum Grav.* **29** 065005

[30] Smith-Lefebvre N, Ballmer S, Evans M, Waldman S, Kawabe K, Frolov V and Mavalvala N 2011 Optimal alignment sensing of a readout mode cleaner cavity *Opt. Lett.* **36** 4365

[31] Bertolini A, DeSalvo R, Galli C, Gennaro G, Mantovani M, Márka S, Sannibale V, Takamori A and Torrie C I 2006 Design and prototype tests of a seismic attenuation system for the advanced-LIGO output mode cleaner *Class. Quantum Grav.* **23** 111–8

[32] DeRosa R *et al* 2012 Global feed-forward vibration isolation in a km scale interferometer *Class. Quantum Grav.* **29** 215008

[33] Levin Y 1998 Internal thermal noise in the LIGO test masses: a direct approach *Phys. Rev.* D **57** 659–63

[34] Harry G M *et al* 2006 Thermal noise from optical coatings in gravitational wave detectors *Appl. Opt. IP* **45** 1569–74

[35] Buonanno A and Chen Y 2001 Optical noise correlations and beating the standard quantum limit in advanced gravitational-wave detectors *Class. Quantum Grav.* **18** 95–101

[36] Finn L S and Chernoff D F 1993 Observing binary inspiral in gravitational radiation: one interferometer *Phys. Rev.* D **47** 2198–219

[37] Abadie J *et al* 2012 Sensitivity achieved by the LIGO and Virgo gravitational wave detectors during LIGO's sixth and Virgo's second and third science runs *Phys. Rev.* D **85** 122007

[38] Chatterji S, Blackburn L, Martin G and Katsavounidis E 2004 Multiresolution techniques for the detection of gravitational-wave bursts *Class. Quantum Grav.* **21** 1809–18

[39] Chattergi S K 2005 The search for gravitational wave bursts in data from the second LIGO science run *PhD Thesis* Massachusetts Instititute of Technology

[40] Macleod D M *et al* 2012 Reducing the effect of seismic noise in LIGO searches by targeted veto generation *Class. Quantum Grav.* **29** 055006

[41] Smith J R *et al* 2011 A Hierarchical method for vetoing noise transients in gravitational-wave detectors *Class. Quantum Grav.* **28** 235005

[42] Isogai T, The LIGO Scientific Collaboration and The Virgo Collaboration 2010 Used percentage veto for LIGO and virgo binary inspiral searches *J. Phys.: Conf. Ser.* **243** 012005

[43] Daw E J, Giaime J A, Lormand D, Lubinski M and Zweizig J 2004 Long term study of the seismic environment at LIGO *Class. Quantum Grav.* **21** 2255–73

[44] Manson G and de Visme G H 2002 The frequency spectrum of Barkhausen noise *J. Phys. D: Appl. Phys.* **5** 1389–95

[45] Weiss R March 2006 Notes on Barkhausen noise *Technical Report* LIGO-T080355 LIGO Laboratory

[46] Prijatelj M *et al* 2012 The output mode cleaner of GEO 600 *Class. Quantum Grav.* **29** 055009

[47] Smith-Lefebvre N D 2012 Techniques for improving the readout sensitivity of gravitational wave antennae *PhD Thesis* Massachusetts Institute of Technology

[48] Coughlin M W 2010 Noise line identification in LIGO S6 and Virgo VSR2 *J. Phys.: Conf. Ser.* **243** 012010

[49] Robinson C, Sathyaprakash B and Sengupta A 2008 Geometric algorithm for efficient coincident detection of gravitational waves *Phys. Rev.* D **78** 062002

[50] Allen B 2005 A χ^2 time-frequency discriminator for gravitational wave detection *Phys. Rev.* D **71** 062001

[51] Ajith P *et al* 2014 Instrumental vetoes for transient gravitational-wave triggers using noise-coupling models: the bilinear-coupling veto *Phys. Rev.* D **89** 122001

[52] Dergachev V 2005 Description of PowerFlux algorithms and implementation *Technical Report* T050186

[53] Dergachev V 2011 Description of PowerFlux 2 algorithms and implementation *Technical Report* T1000272

[54] Aasi J *et al* 2014 Improved upper limits on the stochastic gravitational-wave background from 2009–2010 Ligo and Virgo data *Phys. Rev. Lett.* **113** 231101

[55] Abadie J *et al* 2012 Upper limits on a stochastic gravitational-wave background using LIGO and Virgo interferometers at 600–1000 Hz *Phys. Rev.* D **85** 122001

[56] Thrane E, Christensen N and Schofield R M S 2013 Correlated magnetic noise in global networks of gravitational-wave detectors: observations and implications *Phys. Rev.* D **87** 123009

[57] Aasi J *et al* 2013 Enhanced sensitivity of the LIGO gravitational wave detector by using squeezed states of light *Nat. Photonics* **7** 613–9

[58] The Virgo collaboration and The LIGO Scientific Collaboration 2013 Prospects for localization of gravitational wave transients by the Advanced LIGO and Advanced Virgo observatories in preparation

[59] Essick R, Blackburn L and Katsavounidis E 2013 Optimizing vetoes for gravitational-wave transient searches *Class. Quantum Grav.* **30** 155010

[60] Biswas R *et al* 2013 Application of machine learning algorithms to the study of noise artifacts in gravitational-wave data *Phys. Rev.* D **88** 062003

[61] Abbott B P *et al* 2011 Implementation and testing of the first prompt search for gravitational wave transients with electromagnetic counterparts *Astron. Astrophys.* **539** A124

[62] Evans P A *et al* 2012 Swift follow-up observations of candidate gravitational-wave transient events *Astrophys. J.* **203** 28

[63] Abadie J *et al* 2010 Predictions for the rates of compact binary coalescences observable by ground-based gravitational-wave detectors *Class. Quantum Grav.* **27** 173001